

1 Calibration of Strain Gauged Square Tunnels for Centrifuge 2 Testing

3
4 **Grigorios Tsinidis^a, Charles Heron^b, Gopal Madabhushi^c, Kyriazis Pitilakis^a**

5
6 ^a Aristotle University, Department of Civil Engineering, Thessaloniki, Greece

7 ^b University of Nottingham, Faculty of Engineering, Nottingham, UK

8 ^c University of Cambridge, Schofield Centre, Cambridge, UK

9
10 **Corresponding author:** Grigorios Tsinidis, Dr. Civil Engineer, MSc, Department of Civil
11 Engineering, Research Unit of Geotechnical Earthquake Engineering and Soil Dynamics,
12 Aristotle University of Thessaloniki, PO BOX 424 GR-54124, Thessaloniki, Greece, tel:
13 +302310994208, e-mail: gtsinidi@civil.auth.gr

14
15 **Abstract:** A series of dynamic centrifuge tests was conducted on square aluminum tunnel-
16 models embedded in dry sand. The tests were carried out at the Schofield Centre of the
17 Cambridge University Engineering Department, aiming to investigate the dynamic response
18 of these type of structures. An extensive instrumentation scheme was employed to record the
19 soil-tunnel system response, which comprised of miniature accelerometers, total earth
20 pressures cells and position sensors. To record the lining forces, the model tunnels were strain
21 gauged. The calibration of the strain gauges, the data from which was crucial to furthering our
22 understanding on the seismic performance of box-type tunnels, was performed combining
23 physical testing and numerical modelling. This technical note summarizes this calibration
24 procedure and highlighting the importance of advanced numerical simulation in the
25 calibration procedure of complex construction models.

26
27 **Keywords:** Centrifuge modelling; Calibration; Strain Gauges; Numerical analysis

28 29 1. Introduction

30 Large underground structures (e.g. subways, metro stations, underground parking lots, utility
31 tunnels) have a vital socio-economic role - being a crucial part of the transportation and utility
32 networks in an urban area. To prevent disruption arising from earthquake induced damage,
33 rigorous seismic design procedures need to be developed, verified and implemented. In this

34 context a range of different experimental researches have been carried out over recent years
35 aiming at the investigation of the seismic response of underground structures and tunnels
36 (Shabayama et al., 2010, Lanzano et al., 2012; Cilingir and Madabhushi, 2011a, 2011b,
37 2011c; Chian and Madabhushi, 2011; Chen et al., 2013; Chen and Shen, 2014; Tsinidis et al.,
38 2015a; Ulgen et al., 2015; Abuhajar et al., 2015). Experimental studies have been also
39 conducted for the evaluation of the seismic behavior of actual case studies during retrofitting
40 projects (Adalier et al., 2003; Chou et al., 2010). Although there are some published
41 experimental programs investigating the behaviour of rectangular embedded structures, where
42 strain gauges were employed to record the lining forces (e.g. Chen and Shen, 2014), no clear
43 reference is given for the calibration of these crucial instruments.

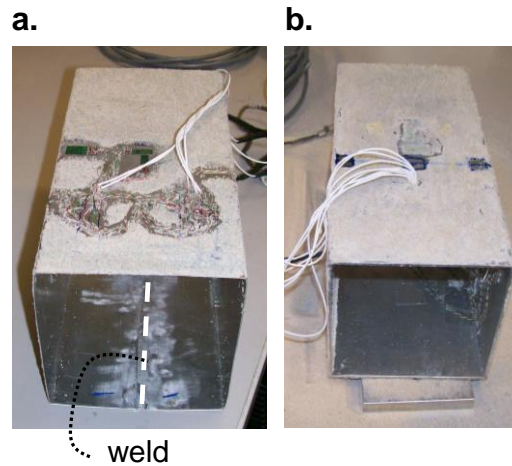
44 This lack of reference, along with the need for more artificial ‘case studies’, motivated the
45 realisation of the collaborative experimental project TUNNELSEIS, through the EU funded
46 research project SERIES. Within the framework of this research project, the seismic response
47 of shallow square tunnels embedded in dry sand was investigated by means of dynamic
48 centrifuge tests. The tests were carried out at the geotechnical centrifuge facility of the
49 Schofield Centre, University of Cambridge. This technical note summarizes the calibration
50 procedure followed for the resistance strain gauges, which were used to record the lining
51 forces and highlighting the significance of advanced numerical simulation in the calibration
52 procedure of complex construction models.

53

54 **2. Description of centrifuge tests undertaken**

55 Three dynamic centrifuge tests were performed on square tunnel models embedded in dry
56 Hostun HN31 sand, reconstituted at two different relative densities of about 50 % and 90 %.

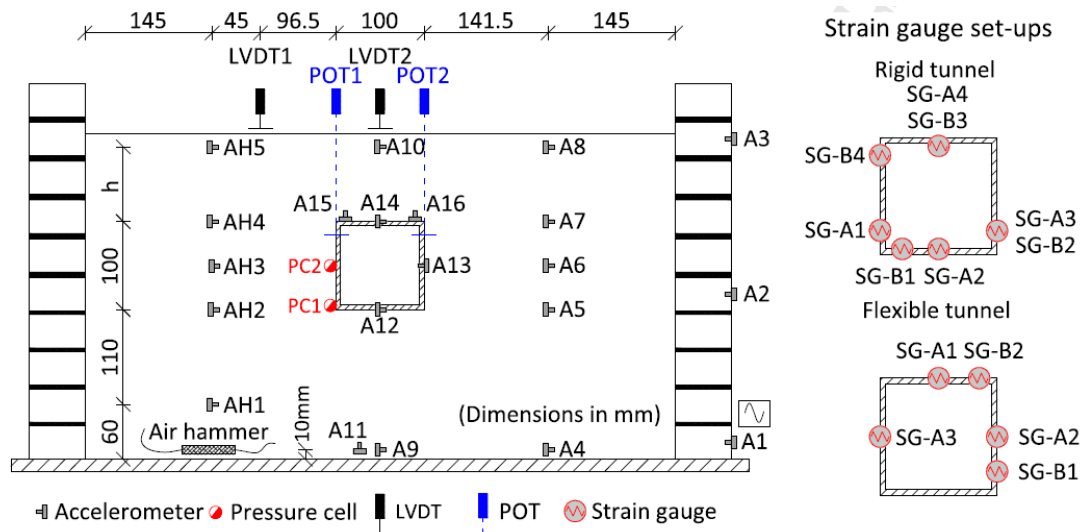
57 Two square tunnel models were manufactured and tested, namely: a relative rigid one
58 having a thickness of 2 mm and a more flexible one having a thickness of 0.5 mm (Fig. 1).
59 The rigid model was made of an extruded section of 6063A aluminum alloy, while the
60 flexible model was manufactured by folding a 33swg soft aluminum foil to form the square
61 section and joined by means of a weld at the centre of the invert slab of the tunnel. Both the
62 models were 100 mm wide, while the length was 220 mm for the rigid model and 210 mm for
63 the flexible one. The thickness of the linings was selected so as to study the effects of tunnel
64 flexibility at extreme ends. To simulate more realistically the soil-structure interface, Hostun
65 sand was stuck to the external face of the tunnel-models, creating a rough surface.



66
67 **Fig. 1.** (a) Flexible tunnel, (b) Rigid tunnel

68

69 A typical model layout is presented in **Fig. 2**. A dense instrumentation scheme was
70 implemented to record the soil-tunnel systems response, comprising of miniature
71 accelerometers, linear variable differential transformers (LVDTs), draw wire potentionmeters
72 (POTs), miniature total earth pressure cells (PCs) and resistance strain gauges to measure the
73 internal forces of the lining at several locations (axial and bending moment strains). Details
74 about the model preparation, setups, and representative experimental data may be found in
75 [Tsinidis et al. \(2014; 2015b; 2015c\)](#).



76
77 **Fig. 2.** Typical models layout (h = 60 mm for flexible tunnel, 100 mm for rigid tunnel)

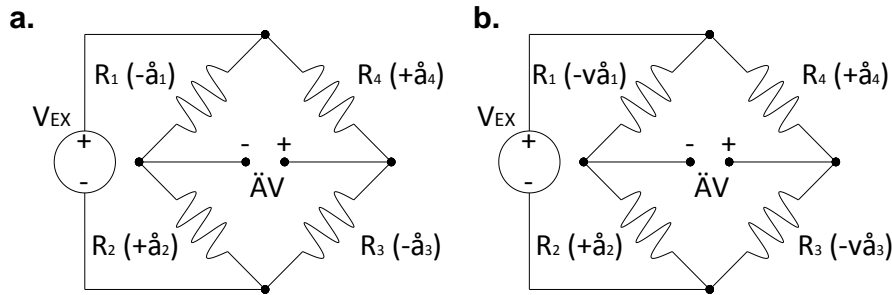
78

79 3. Strain gauging regime

80 Resistance strain gauges (TML FLA-6-350-23) were attached to the inner and outer face of
81 the tunnels to measure the bending moment and the axial force (bending and axial strains) at
82 several locations around the tunnel lining (**Fig. 2**). Eight sets of gauges were used for the rigid

83 tunnel, with four of them recording the bending moments near the tunnel corners and at the
 84 middle of the roof slab (SG-B1, SG-B2, SG-B3 and SG-B4 in Fig. 2) and four of them
 85 recording the axial forces in the walls and the slabs of the model tunnel (SG-A1, SG-A2, SG-
 86 A3, SG-A4 in Fig. 2). Similarly, five sets of strains gauges were used for the flexible tunnel,
 87 namely; two sets were recording the bending moments near the tunnel corners (SG-B1, SG-
 88 B2 in Fig. 2) and three sets were recording the axial forces in the walls and the roof slab (SG-
 89 A1, SG-A2, SG-A3 in Fig. 2).

90 To achieve the greatest possible accuracy full Wheatstone bridges were used with two
 91 gauges on the inside of the tunnel and two on the outside (Fig. 3). A full bridge allows for
 92 strains which arise from alternative sources to be removed, for example the effect of
 93 temperature changes, axial forces (in the case of the bending gauges) and bending moments
 94 (in the case of the axial gauges).



95
 96 **Fig. 3.** Typical circuit layouts for (a) bending moment strain gauges, (b) axial force strain gauges
 97

98 The normal procedures with regard to adhering the gauges to the tunnel were followed. In
 99 particular, to record the lining bending moments, the gauges were arranged by attaching a pair
 100 of arms on the external face of the lining (e.g. R₁ and R₃ in Fig. 3a) and a second pair on the
 101 internal face (e.g. R₂ and R₄ in Fig. 3a). An application of an excitation Voltage V_{ex} at the
 102 extremities of the circuit causes a Voltage variation ΔV that can be measured with a
 103 galvanometer, as illustrated in Fig. 3. According to the wiring pattern, the Voltage ratio is
 104 proportional to the average deformation ε of the gauges:

$$105 \quad \frac{\Delta V}{V_{ex}} = \frac{K_{gf}}{4} \varepsilon = \frac{K_{gf}}{4} (-\varepsilon_1 + \varepsilon_2 - \varepsilon_3 + \varepsilon_4) \quad (1)$$

106 where: K_{gf} is the gauge factor and ε_i is the deformation of the i^{th} arm of the bridge.
 107 Assuming a linear elastic response for the lining, the deformations of the arms may be
 108 computed, as follows:

$$109 \quad \varepsilon_1 = \varepsilon_3 = \frac{N}{EA} + \frac{M}{EI} \times \frac{t}{2}, \quad \varepsilon_2 = \varepsilon_4 = \frac{N}{EA} - \frac{M}{EI} \times \frac{t}{2} \quad (2)$$

110 where: t is the thickness of the lining, EI is the flexural stiffness of the lining, EA is the axial
 111 stiffness of the lining, M is the bending moment at the specific location of the lining and N is
 112 the axial load at the specific location of the lining. By substituting the arm deformations in
 113 Eq. 1, the following expression is obtained for the Voltage change:

$$114 \quad \left\{ \frac{\Delta V}{V_{ex}} \right\}_M = -K_{gf} \times \frac{M}{EI} \times \frac{t}{2} = K_m \times M \quad (3)$$

115 Eq. 3 implies that the measured Voltage ΔV is directly proportional to the bending moment
 116 at the specific section, through the calibration factor K_m and the input Voltage V . In this
 117 regard, it is related to known geometrical and mechanical parameters of the model.

118 Another bridge arrangement was implemented for the axial force strain gauges (Fig. 3b). A
 119 pair of gauges (R_2 and R_4) was attached in the circumferential direction, while a second pair
 120 of gauges (R_1 and R_3) was aligned perpendicularly, in order to form a couple of Poisson's
 121 gauges. Following the elastic theory, the arm deformations are now given by the following
 122 expressions:

$$123 \quad \begin{aligned} \varepsilon_1 &= -\nu \left(\frac{N}{EA} + \frac{M}{EI} \times \frac{t}{2} \right), & \varepsilon_2 &= \frac{N}{EA} + \frac{M}{EI} \times \frac{t}{2}, \\ \varepsilon_3 &= -\nu \left(\frac{N}{EA} - \frac{M}{EI} \times \frac{t}{2} \right), & \varepsilon_4 &= \frac{N}{EA} - \frac{M}{EI} \times \frac{t}{2} \end{aligned} \quad (4)$$

124 where: ν the Poison ratio of the aluminium model. By substituting again the arm deformations
 125 in Eq. 1, the following expression is obtained for the Voltage change:

$$126 \quad \left\{ \frac{\Delta V}{V_{ex}} \right\}_N = (1 + \nu) \times \frac{K_{gf}}{2} \times \frac{N}{EA} = K_n \times N \quad (5)$$

127 Similar to the bending moment gauges, the measured ΔV is directly proportional to the axial
 128 force at the specific section through the calibration factor K_n and the input Voltage V .

129

130 **4. Calibration procedure**

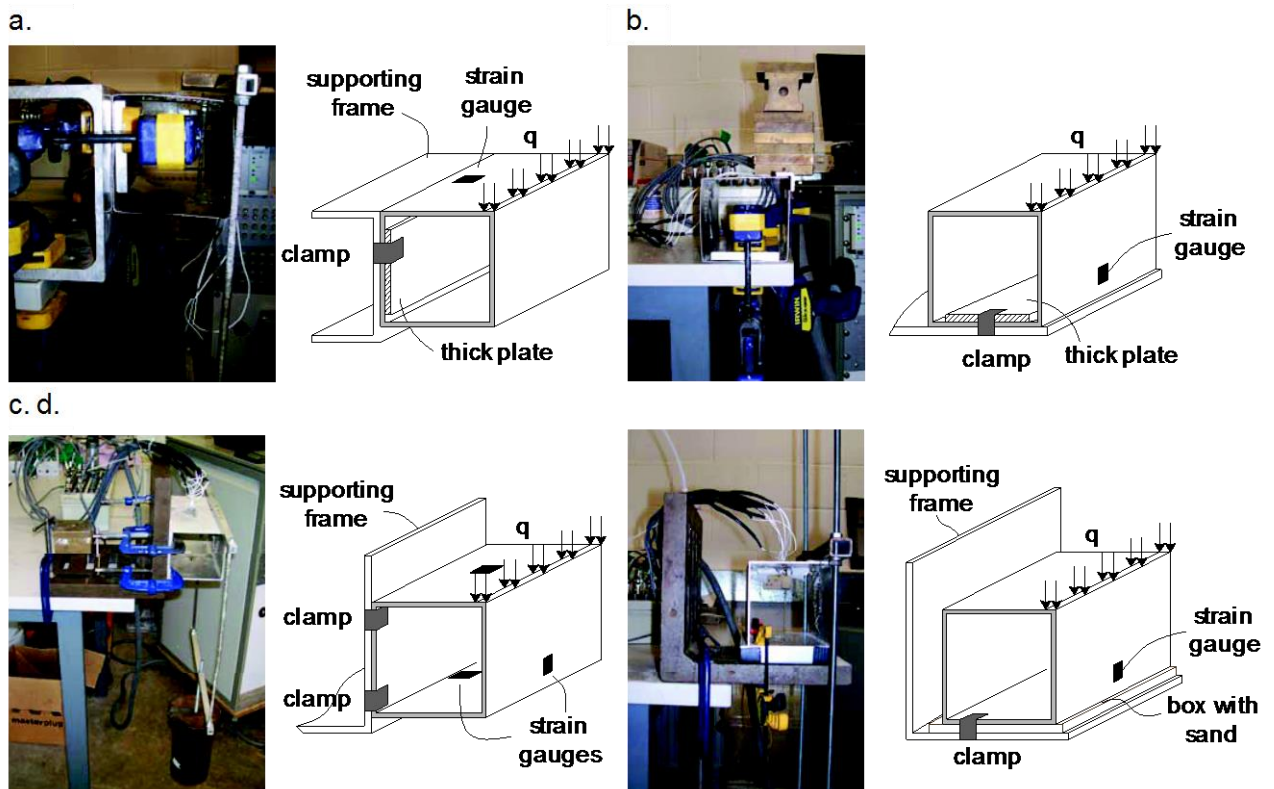
131 The calibration factors for both the axial and the bending moment strain gauges were derived
 132 for simple static loading patterns. For each loading case, the model was incrementally loaded
 133 and unloaded by adding and removing weights, while the output Voltage from each strain
 134 gauge bridge was recorded for each loading step. The loading systems (e.g. loading locations,
 135 fixities) were selected to ensure the elastic response of the model tunnels and therefore they
 136 were slightly different between the flexible and the rigid tunnel, as described in the following
 137 sections. Through these procedures, Voltage-mass calibration curves were derived. To come

138 out with the final internal force-Voltage calibration curves and thus with the final calibration
 139 factors, the static configurations were properly simulated and analyzed, by means of 3D static
 140 analyses, using the general purpose finite element code ABAQUS (ABAQUS, 2012). This
 141 numerical approach was selected due to the complicated nature of the calibration system that
 142 could not be described by available closed form solutions.

143

144 4.1 Flexible tunnel loading regime

145 **Figures 4a** and **4b** present the loading set ups used for the calibration of the bending moment
 146 and axial force strain gauges of the flexible tunnel, respectively.



147

148 **Fig. 4.** Static configurations for the calibration of (a) the bending moment gauges of the flexible
 149 tunnel, (b) the axial force gauges of the flexible tunnel, (c) the bending moment gauges of the stiff
 150 tunnel, (d) the axial force gauges of the stiff tunnel

151

152 To calibrate the bending moment strain gauges, one tunnel wall was clamped to a rigid
 153 frame. The loading was introduced on the free side of the tunnel using a frame (to distribute
 154 the load along the length of the tunnel), consequently forming a ‘cantilever static system’ for
 155 the wall containing the strain gauge being calibrated (**Fig. 4a**). A thick aluminum plate was
 156 introduced between the clamps and the tunnel to avoid stress concentrations in the tunnel

157 lining near the connections that could cause local yielding. This configuration resulted in a
158 fixed connection for almost the entirety of the tunnel wall.

159 A similar configuration was used for the calibration of the axial force strain gauges (Fig.
160 4b). The tunnel base slab was fixed using clamps, while a thick aluminum plate was
161 introduced between the clamps and the tunnel to avoid stress concentrations near the fixities,
162 similar to the bending moment case. The loading was introduced along the upper edge of the
163 wall containing the strain gauge under calibration.

164 Each loading-unloading procedure was performed twice, so as to check the repeatability of
165 the gauges response, while to calibrate all the strain gauges, the tunnel was appropriately
166 rotated and clamped for each case. The calibration procedure was performed before the main
167 centrifuge test, while no post test calibration was performed, as the tunnel collapsed during
168 the actual test (Tsinidis et al., 2015b).

169

170 **4.2 Rigid tunnel loading regime**

171 Figures 4c and 4d present the loading set ups used for the calibration of the bending moment
172 and axial force strain gauges of the rigid tunnel. To calibrate the bending moment strain
173 gauges, one tunnel wall was clamped using four points (upper and lower corner at each end)
174 to a rigid frame (Fig. 4c). The loading was introduced on the free side of the tunnel using a
175 frame. This configuration allowed the calibration of all the bending moment strain gauges
176 simultaneously. The loading-unloading procedure was performed twice to check the
177 repeatability of the gauges response, while the model was re-clamped and loaded several
178 times, changing each time the “fixed side wall”. This procedure allowed multiple records for
179 different loading patterns for each strain gauge to be collated.

180 A set-up similar to the flexible tunnel configuration was used for the calibration of the
181 axial force strain gauges (Fig. 4d). The tunnel was seated on a small box containing
182 compacted sand, while the base slab was held down (in case of uplifting during loading) with
183 clamps at both ends of the tunnel. The solution involving the sand box at the base of the
184 tunnel was implemented due to the sand that had been stuck along the external face of the
185 tunnel, which in addition to the relatively high rigidity of the tunnel lining would have
186 resulted to stress concentrations (e.g. ‘stress bridging’) affecting the strain gauge recording
187 response, if a rigid flat surface (as in the case of the flexible tunnel) had been used under the
188 tunnel instead. Indeed, testing the gauges without the sand box at the base did result in a much
189 more scattered response. The loading was introduced upon the wall containing the under
190 calibration strain gauge.

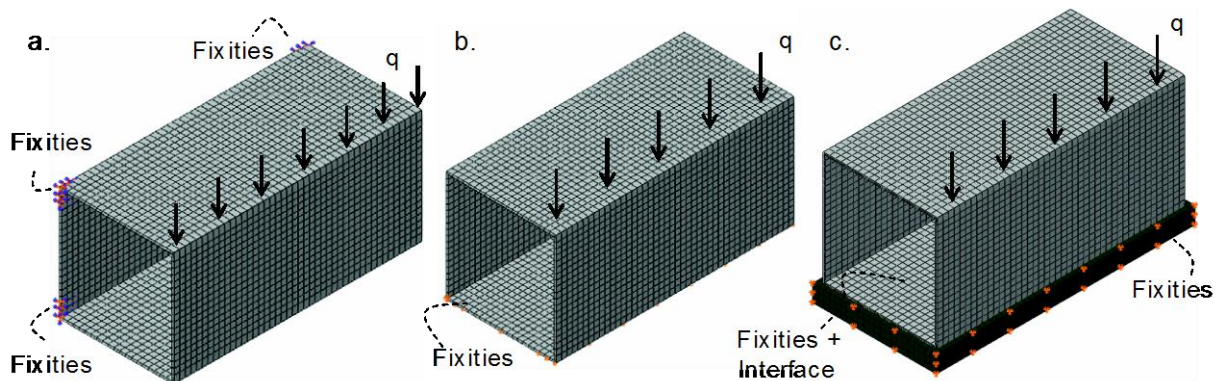
191 Similar to the other cases, each loading-unloading procedure was performed twice, so as to
192 check the repeatability of the gauges response, while to calibrate all the strain gauges, the
193 tunnel was properly rotated and clamped for each case. Both pre- and post-test calibration was
194 performed to check the repeatability of the gauges response. Care was taken during the
195 calibration procedure to ensure the loading magnitude was sufficient to obtain clear
196 measurements of the strains without causing any yielding of the model-tunnel.

197

198 4.3 Numerical analysis

199 The internal forces at each gauge position were computed through numerical static analyses of
200 the structural models. The results were plotted against the measured voltage change in order
201 to evaluate each gauge calibration factor. The structural models were simulated in ABAQUS
202 (ABAQUS, 2012) with elastic shell elements, taking into account the exact supports and
203 loading positions of each test case (Fig. 5). The static load caused by the weight was
204 introduced on the loaded area of the tunnel lining as an equivalent pressure, q , thus
205 resembling the actual loading configuration imposed during the calibration procedure.

206



207

208 **Fig. 5.** (a) Numerical model of the rigid tunnel bending moment strain gauges calibration
209 configuration, (b) simplified numerical model of the rigid tunnel axial strain gauges calibration
210 configuration, (c) rigorous numerical model of the rigid tunnel axial strain gauges calibration
211 configuration

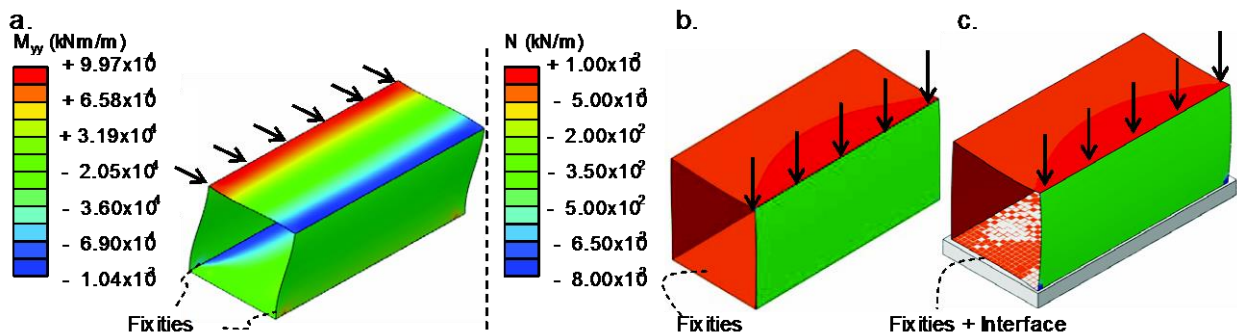
212

213 The precise simulation of the actual support system by the numerical analyses is the key in
214 order to determine the most accurate value for the internal force at the strain gauge locations.
215 To replicate the static system used during the calibration procedure of the flexible tunnel
216 bending moment strain gauges, the translational and rotational degrees of freedom of the
217 tunnel along the clamped area (restrained with the thick aluminum plate as discussed) were
218 fixed, while a similar procedure was also used for the axial force strain gauges.

219 For the simulation of the bending moment strain gauges calibration procedure of the stiff
 220 tunnel, both the transnational and rotational degrees of freedom of the clamped areas were
 221 fixed (Fig 5a). To examine the effect of the sand box at the base of the tunnel (used during the
 222 calibration of the axial force strain gauges) two cases were investigated; during the first case,
 223 the base slab of the tunnel was simply fixed in terms of vertical displacement (Fig. 5b), while
 224 in the second case the sand layer under the tunnel was also simulated with solid elements
 225 (Fig. 5c). The sand-tunnel interface was adequately modelled using a finite-sliding hard
 226 conduct formulation embedded in ABAQUS (ABAQUS, 2012). The model precludes
 227 penetration between the interacting surfaces, while it allows for separation. The tangential
 228 behaviour was simulated implementing the classical isotropic Coulomb friction model. The
 229 friction coefficient μ was set equal to 0.62, based on the friction angle of the specific sand
 230 fraction. The restraints that were induced by the clamps (e.g. end sides) were simulated with
 231 proper kinematic constrains between the model tunnel nodes and the base of the sand layer
 232 model. The sand elastic properties were parametrically checked, ranging between values
 233 corresponding to either loose or dense sand.

234 Fig. 6 portrays typical deformed shapes of the stiff model tunnel, along with the
 235 distributions of the internal forces for pressure loadings corresponding to a 1 kilogram of
 236 weight. The effect of the static model configuration on the axial force of the stiff tunnel is
 237 highlighted by comparing the numerical predictions between the simplified model and the
 238 detailed model (Figs. 6b and c). The presented results refer to a relatively loose sand bed.
 239 Generally, the difference on the computed axial force between the more accurate and the
 240 simple model was less than 5 %, indicating that the presence of the sand bed did not had a
 241 significant impact on the simulation.

242

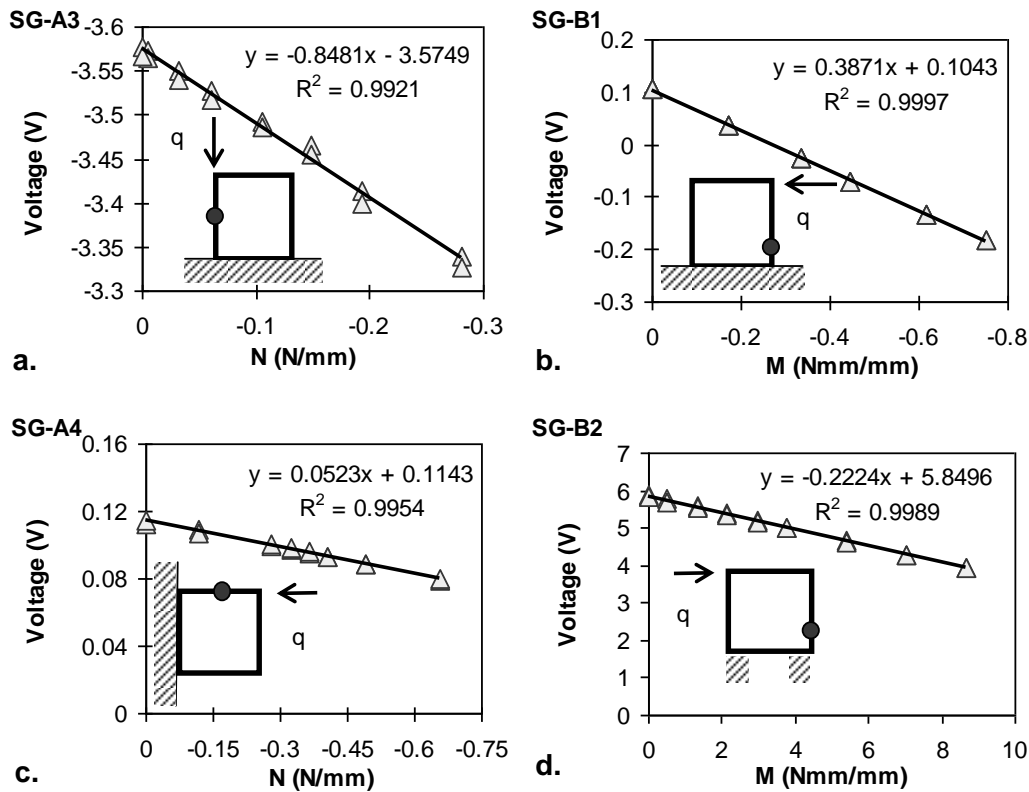


243

244 **Fig. 6.** Representative deformed shapes of the stiff tunnel for different loading configurations, (a)
 245 contour diagram tunnel bending moment M_{yy} , (b) contour diagram of the axial force computed by the
 246 simplified model, (c) contour diagram of the axial force computed by the detailed model

247 **4.4 Calibration factors**

248 **Fig. 7** presents representative examples of Voltage-internal force calibration curves, for axial
 249 force and bending moment strain gauges attached to both the flexible and the rigid tunnel.

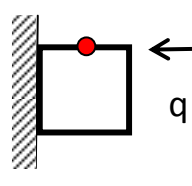
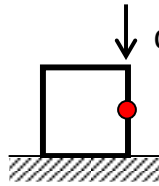
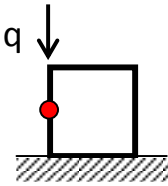


250
 251 **Fig. 7.** Voltage-internal force calibration curves for the flexible tunnel strain gauges (a, b) and the
 252 rigid tunnel strain gauges (c, d)

253
 254 **Tables 1 and 2** summarize the calibration factors estimated for the flexible tunnel, while in
 255 **Tables 3 and 4** the calibration factors of the rigid tunnel strain gauges are presented. With
 256 regard to the flexible tunnel, the comparisons between the different loading repetitions
 257 reveal differences up to 4-5 % for the bending moment strain gauges and up to 30 % for the
 258 axial force strain gauges. Similar observations are made regarding the differences between the
 259 recorded responses of the rigid tunnel strain gauges.

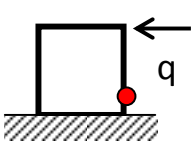
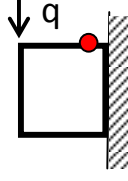
260 Generally, the calibration factors of the axial strain gauges were found to be more scattered
 261 compared to the bending moment strain gauges. This is attributed to difficulties regarding the
 262 axial loading of the tunnel-models. As already stated, the loading should be ‘strong’ enough
 263 to obtain clear measurements of the axial strains, without however, jeopardizing the elastic
 264 response of the model (e.g. yielding). In addition, problems related to the support systems
 265 used during the calibration procedure or stress concentrations caused by the sand stuck around
 266 the tunnel could affect the estimated factors.

267 **Table 1.** Axial force strain gauge calibration factors for the flexible tunnel

Loading case							Final calibration factor N/mm
	1	2	1	2	1	2	
Repetition #	1	1	2	1	2	-	
SG-A1	-1.5	-	-	-	-	-1.5	
SG-A2*	-	9.7	3.2	-	-	3.2	
SG-A3	-	-	-	-1.2	-1.7	-1.4	

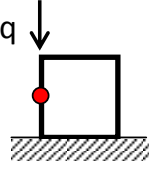
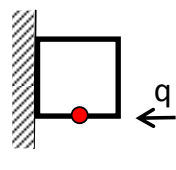
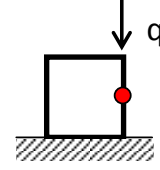
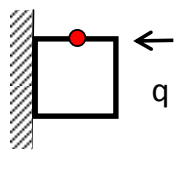
268 * probably malfunctioned

269 **Table 2.** Bending moment strain gauge calibration factors for the flexible tunnel

Loading case					Final calibration factor Nmm/mm
	1	2	1	2	
Repetition #	1	2	1	2	-
SG-B1	2.50	2.58	-	-	2.54
SG-B2	-	-	2.69	2.70	2.70

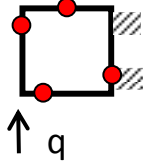
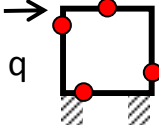
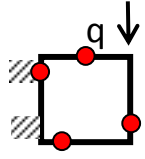
270

271 **Table 3.** Axial force strain gauge calibration factors estimated before and after test for the rigid tunnel
 272 (factor for pre test calibration procedure / factor for post test calibration procedure)

Loading case										Final calibration Factors (N/mm)	
	1	2	1	2	1	2	1	2	3	Pre test	Post test
SG-A1	24.8/ 19.6	24.0/ 22.0	-	-	-	-	-	-	-	24.4	20.8
SG-A2	-	-	15.8/ 17.1	18.6/ 26.0	-	-	-	-	-	17.2	21.6
SG-A3	-	-	-	-	14.6/ 18.5	16.1/ 14.3	-	-	-	15.3	16.4
SG-A4	-	-	-	-	-	-	17.0/ 24	19.1/ 25	15.9/ -	17.3	25

273

274 **Table 4** Bending moment gauges calibration factors estimated before and after test for the rigid tunnel
 275 (factor for pre test calibration procedure / factor for post test calibration procedure)

Calibration factors							Final calibration factors (Nmm/mm)	
	1	2	1	2	1	2	Pre test	Post test
SG-B1	4.50/ 4.50	4.60/ 4.00	4.90/ 4.90	5.10/ 5.20	4.70/ 5.40	4.70/ 5.40	4.74	4.90
SG-B2	-4.90/ -5.20	-5.00/ -5.00	-4.50/ -4.80	-4.60/ -4.90	-4.50/ -4.90	-4.50/ -4.90	-4.66	-4.94
SG-B3*	0.10/ 3.20	0.10/ 3.20	0.10/ 9.00	0.10/ 10.30	-1.40/ -26.00	-1.10/ -23.00	-	-
SG-B4	4.30/ 4.60	4.30/ 4.60	4.70/ 4.50	4.70/ 4.90	5.00/ 5.40	5.20/ 5.40	4.71	4.92

276 *broken

277

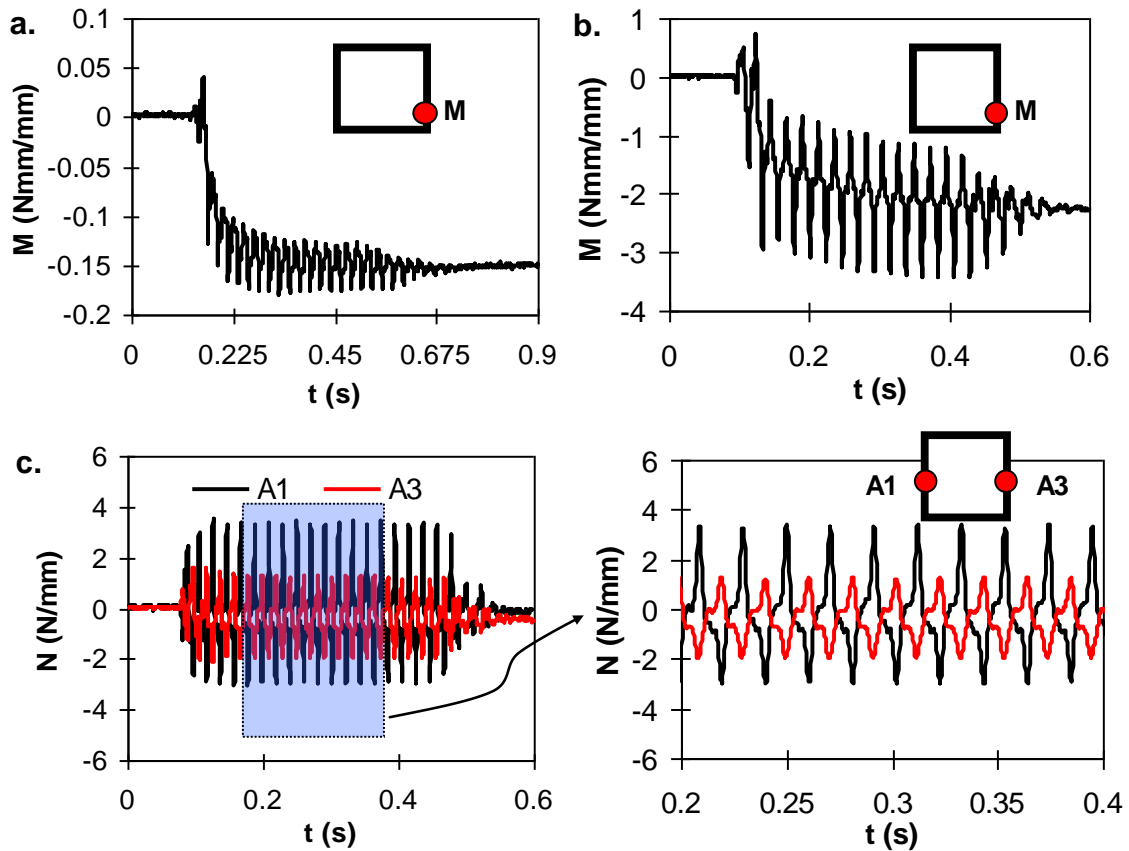
278 The calibration factors derived after the main centrifuge tests (for the rigid tunnel) were
 279 slightly higher compared to the pre-test values, with the deviations being larger for the axial
 280 force gauges. This could be attributed to a permanent lining response as a consequence of
 281 severe loading during the earthquake loading. Therefore, the pre-test calibration factors were
 282 adopted for the final interpretation of the lining recorded response data. In particular, a mean
 283 value was adopted for each gauge factor, accounting for all the estimated factors of each
 284 strain gauge and assuming the same level of uncertainty for each loading procedure.

285

286 5. Representative records

287 **Figures 7a and 7b** illustrate representative time histories of the dynamic bending moments,
 288 recorded near the right side-wall bottom corner of both the flexible and the rigid tunnels.
 289 Positive values represent bending moment with tensile stress increments for the internal lining
 290 face. Records indicate significant locked-in bending induced strain after shaking finished, due
 291 to the soil densification and yielding around the tunnel. Representative dynamic axial force
 292 time histories recorded at the side-walls of the rigid tunnel are presented in **Fig. 7c**. In this
 293 case, positive values represent tensile axial force. The records are out of phase, indicating a
 294 rocking mode of vibration for the tunnel in addition to the pure racking distortion. A thorough

295 discussion of the recorded response may be found in relevant publications (e.g. Tsinidis et al.,
296 2014, 2015b; 2015c).



297
298 **Fig. 8.** Dynamic bending moment time histories recorded near the right side-wall bottom corner of the
299 (a) flexible and the (b) rigid tunnel, (c) dynamic axial force time histories recorded on the side-walls of
300 the rigid tunnel

301

302 6. Conclusions

303 A series of dynamic centrifuge tests were performed on square model tunnels embedded in
304 dry sand. This technical note presented the calibration procedure followed for the resistance
305 strain gauges, which were attached to the model tunnels to record the lining internal forces at
306 several crucial locations during the tests. Strain gauge calibration factors were derived for
307 simple static loading patterns. A crucial step within this calibration procedure was the rational
308 evaluation of the model response due to these simplified loading patterns (e.g. computation of
309 internal forces at strain gauge locations). This evaluation was performed by means of 3D
310 numerical analysis of the static configurations, simulating as accurately as possible the
311 supports and loading regimes. Accounting for the complicated nature of the calibration
312 system and the inexistence of plausible analytical closed form solutions, numerical analysis

313 was mandatory. The combination of experimental testing and numerical analysis was found to
314 be quite satisfactorily in calibration of this model, as the recorded lining forces were found to
315 be in good agreement with the theoretically expected behaviour. The main conclusion of this
316 work is that combined experimental testing and numerical analysis can be used quite
317 efficiently for the calibration of complex structural models, as well as for cases where no
318 analytical closed form solutions are available. A crucial point for the efficiency of this
319 approach is the proper simulation of the static configurations (e.g. supports, loading regimes
320 etc).

321

322 **Acknowledgements**

323 The research leading to these results has received funding from the European Community's
324 Seventh Framework Programme [FP7/2007-2013] for access to the Turner Beam Centrifuge,
325 Cambridge, UK under grant agreement n° 227887 [SERIES: Seismic Engineering Research
326 Infrastructures for European Synergies; www.series.upatras.gr/TUNNELSEIS]. The technical
327 support received by the Technicians of the Schofield Centre is gratefully acknowledged.

328

329 **References**

- 330 ABAQUS (2010) ABAQUS: theory and analysis user's manual version 6.10. Dassault Systèmes
331 SIMULIA Corp, Providence
- 332 Abuhajar O, El Naggar H, Newson T (2015) Seismic soil-culvert interaction. Canadian Geotechnical
333 Journal 52:1-19
- 334 Adalier K, Abdoun T, Dobry R, Phillips R, Yang D, Naesgaard E (2003) Centrifuge modeling for
335 seismic retrofit design of an immersed tube tunnel. International Journal of Physical Modelling on
336 Geotechnics 3(2):23-35
- 337 Chen G, Wang Z, Zuo X, Du X, Gao H (2013) Shaking table test on seismic failure characteristics of a
338 subway station structure in liquefiable ground. Earthquake Engineering and Structural Dynamics
339 42:1489-1507
- 340 Chen ZY, Shen H (2014) Dynamic centrifuge tests on isolation mechanism of tunnels subjected to
341 seismic shaking. Tunnelling and Underground Space Technology 42:67-77
- 342 Chian SC, Madabhushi SPG (2012) Effect of buried depth and diameter on uplift of underground
343 structures in liquefied soils. Journal of Soil Dynamics and Earthquake Engineering 41:181-190
- 344 Chou JC, Kutter BL, Travararou T, Chacko JM (2010) Centrifuge modeling of seismically induced
345 uplift for the BART transbay tube. Journal of Geotechnical and Geoenvironmental Engineering
346 137(8):754-765

347 Cilingir U, Madabhushi SPG (2011a) A model study on the effects of input motion on the seismic
348 behaviour of tunnels. *Journal of Soil Dynamics and Earthquake Engineering* 31:452-462

349 Cilingir U, Madabhushi SPG (2011b) Effect of depth on the seismic response of square tunnels. *Soils*
350 *and Foundations* 51(3):449-457

351 Cilingir U, Madabhushi SPG (2011c) Effect of depth on the seismic response of circular tunnels.
352 *Canadian Geotechnical Journal* 48(1):117-127

353 Lanzano G, Bilotta E, Russo G, Silvestri F, Madabhushi SPG (2012) Centrifuge modeling of seismic
354 loading on tunnels in sand. *Geotechnical Testing Journal* 35(6):10-26

355 Shibayama S, Izawa J, Takahashi A, Takemura J and Kusakabe O (2010) Observed behavior of a
356 tunnel in sand subjected to shear deformation in a centrifuge. *Soils and foundations* 50(2):281-294

357 Tsinidis G, Heron C, Pitilakis K, Madabhushi SPG (2014) Physical modeling for the evaluation of the
358 seismic behavior of square tunnels. In: Ilki A and Fardis M (eds) *Seismic evaluation and*
359 *rehabilitation of structures, Geotechnical Geological and Earthquake Engineering*, 26, Springer
360 International Publishing, Switzerland, pp 389-406

361 Tsinidis G, Rovithis E, Pitilakis K, Chazelas JL (2015a) Dynamic response of shallow rectangular
362 tunnels in sand by centrifuge testing, in: Taucer F, Apostolska R (eds) *Experimental research in*
363 *earthquake engineering - EU-SERIES concluding workshop, Geotechnical Geological and*
364 *Earthquake Engineering*, 35, Springer International Publishing, Switzerland, pp 493-507

365 Tsinidis G, Heron C, Pitilakis K, Madabhushi SPG (2015b) Centrifuge modelling of the dynamic
366 behavior of square tunnels in sand. In: Taucer F and Apostolska R (eds) *Experimental research in*
367 *earthquake engineering - EU-SERIES concluding workshop, Geotechnical Geological and*
368 *Earthquake Engineering*, 35, Springer International Publishing, Switzerland, pp 509-523

369 Tsinidis G, Pitilakis K, Madabhushi G, Heron C (2015c) Dynamic response of flexible square tunnels:
370 centrifuge testing and validation of existing design methodologies. *Geotechnique* 65(5):401-417

371 Ulgen D, Saglam S and Ozkan MY (2015) Dynamic response of a flexible rectangular underground
372 structure in sand: centrifuge modeling. *Bulletin of Earthquake Engineering* 13:2547-2566